

Run stop shock, run shock run: Spontaneous and stimulated gait-switching in a unicellular octoflagellate

Kirsty Y. Wan and Raymond E. Goldstein

Department of Applied Mathematics and Theoretical Physics, Centre for Mathematical Sciences,
University of Cambridge, Wilberforce Road, Cambridge CB3 0WA, United Kingdom

(Dated: June 24, 2017)

In unicellular flagellates, growing evidence suggests control over a complex repertoire of swimming gaits is conferred intracellularly by ultrastructural components, resulting in motion that depends on flagella number and configuration. We report the discovery of a novel, tripartite motility in an octoflagellate alga, comprising a forward gait (*run*), a fast knee-jerk response with dramatic reversals in beat waveform (*shock*), and, remarkably, long quiescent periods (*stop*) within which the flagella quiver. In a reaction graph representation, transition probabilities show that gait switching is only weakly reversible. Shocks occur spontaneously but are also triggered by direct mechanical contact. In this primitive alga, the capability for a millisecond stop-start switch from rest to full speed implicates an early evolution of excitable signal transduction to and from peripheral appendages.

In his *De Incessu Animalium* Aristotle had thus described the walk of a horse [1]: “*the back legs move diagonally in relation to the front legs, for after the right fore leg animals move the left hind leg, and then the left foreleg, and finally the right hind leg.*” The control mechanism of leg activation was unknown to Aristotle, but is now understood to arise from ‘central pattern generators’ [2, 3], which produce electrophysiological signals (action potentials) that drive limbs in a range of spatiotemporal symmetries. While microorganisms achieve motility through microscale analogues of limbs called cilia and flagella, absent a nervous system the mechanism of control must be quite different. Nevertheless, species of unicellular algae are capable of executing patterns of flagellar beating akin to the trot and gallop of quadrupeds [4]. In these cases, the extent of intracellular control of appendages is becoming increasingly evident [4–7].

Here, we detail the discovery of a surprising motility in the octoflagellate marine alga *Pyramimonas octopus* (Fig. 1). Swimming requires coordination of eight flagella in a pseudo-breaststroke, in which diametrically opposed pairs beat largely in synchrony. We find that this forward *run* gait can be interrupted by abrupt episodes involving dramatic changes in flagella beating – hereafter termed *shocks*, which occur spontaneously but can also be induced by external stimuli. Cells also display a distinctive *stop* gait which can be prolonged, where cell body movement is stalled but yet the flagella quiver with minute oscillations. *P. octopus* belongs to a fascinating group of unicellular algae bearing 2^k flagella, which substantiates a delicate interplay between passive fluid mechanics and active intracellular control in the coordination of multiple flagella [4]. Compared to bacteria, the larger size of these algae facilitates visualization, allowing us to demonstrate how flagellar beating leads directly to gait-switching and trajectory reorientation, and to expose the excitable nature of the eukaryotic flagellum.

Cell cultures were obtained from the Scandanavian Collection of Algae and Protozoa (SCCAP K-0001, *P.*

octopus Moestrup et Aa. Kristiansen 1987), and grown in Guillard’s F/2 medium under controlled illumination (14:10 day/night diurnal cycle, at 22°C). Cells are oblong or rectangular in aspect (Fig. 1), with length ($17.05 \pm 1.74 \mu\text{m}$) and width ($9.05 \pm 1.23 \mu\text{m}$). In their vegetative state cells have 8 flagella, each of length comparable to the longitudinal dimension of the cell body, which emerge radially from an apical grove [8]. Imaging was conducted under white light illumination on an inverted microscope (Nikon Eclipse TE2000-U) and high-speed recordings made at up to 3000 fps (Phantom v311, Vision Research). Organisms were harvested during exponential growth (at 10^4 – 10^5 cells/cm³), and 50–150 μl of suspension were pipetted gently into shallow quasi-2D chambers (top + bottom: glass, side: Frame-Seal slide chambers – BIO-RAD) for imaging and precision cell and flagella tracking via custom MATLAB algorithms and IMAGEJ extensions – see Supplemental Materials (SM). We ensured cell viability by minimizing environmental stress responses: acclimating cells prior to observation, and limiting continuous light exposure to $\lesssim 15$ minutes.

When swimming freely, cells spin about their long axis. Restricting to individuals traversing the focal plane, we can observe the flagella distinctly. The *run*, *shock*, and



FIG. 1. *Pyramimonas octopus*. (a) Side and (b) top views (flagella spiral clockwise). Eyespot visible as conspicuous orange organelle. (Scale bar: 5 μm .)

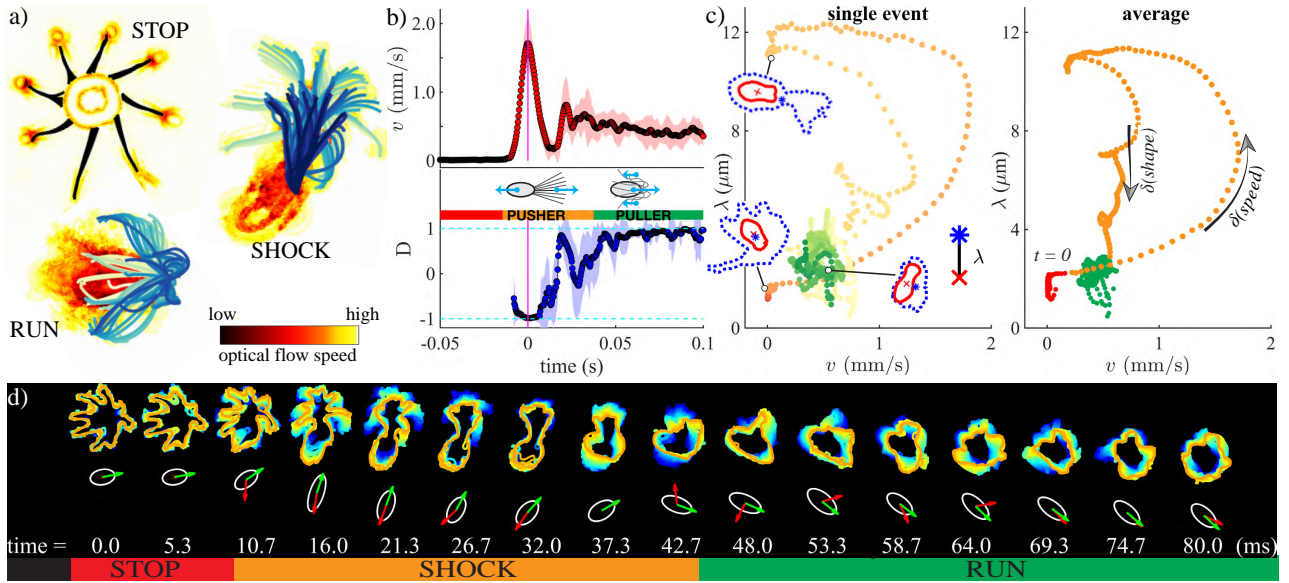


FIG. 2. Three gaits of *P. octopus*. (a) Cell viewed from the TOP (SIDE) during stop (run, shock) gaits. Flagella traced from successive frames are overlaid onto optical flow maps following iso-intensity pixels (pixel flow rate scales with activity). (b) Transition from stop to run occurs via a shock, with rapid changes in speed v and alignment D (‘pusher’ to ‘puller’ transition, shaded = 1 standard deviation). (c) Gaits, and the phase trajectories that connect them, are confined to specific regions of v - λ phase space. (d) Top row: sequence of changes in flagellar beating and cell orientation, plotted here on two timescales (coarse 10 ms, fine: 5 ms). Bottom row: ellipses – cell body, arrows – cell orientation $\hat{\mathbf{e}}_R$ (red), direction of motion $\hat{\mathbf{v}}$ (green).

stop gaits (Fig. 2a) are coincident with the three major modes of beating, respectively (ciliary, flagellar, and quiescent) [9]. Changes in flagellar activity produce gait transitions. However, unlike their bacterial counterparts, eukaryotic flagellar beating is not due to basal rotors but rather a coordinated action of dyneins distributed throughout the axoneme [10]. Forward swimming in *P. octopus* arises from ciliary beating (‘puller’), but during shocks all eight flagella are thrown abruptly in front of the cell where they undulate in sperm-like fashion (‘pusher’). Significant hydrodynamic interactions synchronize the flagella during shocks. These ‘knee-jerk’ reactions last only 20 – 30 ms, and are related to the escape response of *Chlamydomonas* and *Spermatozopsis*. The latter is triggered by intense photo- [11, 12] or mechanical stimuli [13], but last much longer (0.2 – 1.0 s) and do not occur spontaneously. The stop gait has no equivalent in the repertoire of green algae studied so far.

We focus on the stereotypical sequence *stop* \rightarrow *shock* \rightarrow *run*: a cell initiates a run from rest via a shock (Fig. 2b). Defining the instantaneous alignment $D = \hat{\mathbf{v}} \cdot \hat{\mathbf{e}}_R$ between the swimming direction $\hat{\mathbf{v}}$ and the cell body axis $\hat{\mathbf{e}}_R$, the puller-like run ($D = 1$) may be distinguished from the pusher-like shock ($D = -1$). Averaged over 10 cells, the translational speed rises rapidly from zero to a maximum of $1,712 \pm 392 \mu\text{m/s}$, but relaxation to a mean run speed of $428 \pm 64 \mu\text{m/s}$ takes ~ 0.05 s. To separate the flagellar motion from body orientation, we track two dynamically morphing boundaries that are delineated by

image intensity: an inner one for the cell body, and an outer one exterior to the flagella (SM). The lengthscale $\lambda(t) = \left\| \frac{\sum_{\mathbf{x} \in \mathcal{B} \setminus \mathcal{A}} \mathbf{x} / |\mathcal{B} \setminus \mathcal{A}| - \sum_{\mathbf{x} \in \mathcal{A}} \mathbf{x} / |\mathcal{A}|}{\|\cdot\|} \right\|$, measures the physical separation between the flagella and the cell body proper, where $\|\cdot\|$ is the Euclidean norm, $|\cdot|$ the cardinality of a set, and \mathcal{A} , \mathcal{B} are pixels interior of the inner and outer boundaries respectively. Naturally, cells at rest exhibit minimal shape fluctuations. In Fig. 2c, the three states (realized at instants $t = t_1, t_2$, and t_3), localize to specific regions of phase-space. Averaging over multiple events, bifurcations from stops to runs via shocks appear as loops with two distinct branches, one involving rapid changes in *speed*, and the second in *shape* (Fig. 2c).

To estimate the transition probabilities between gaits, we implemented a continuous time Markov model, where the instantaneous speed v was discretized to automate a three-state classification from the empirical tracking data (Fig. 3a). The state variable $X(t)$ takes the values $\{0 = \text{stop}, 1 = \text{run}, 2 = \text{shock}\}$. The transition rate matrix $Q = \{q_{ij}\}$, defined by $q_{ij} = \lim_{\Delta t \rightarrow 0} \mathcal{P}(X(\Delta t) = j | X(0) = i) / \Delta t$ for $i \neq j$ (a time-homogeneous Markov process), and $q_{ii} = -\sum_{j \neq i} q_{ij}$, was estimated to be:

$$Q = \begin{array}{c} \begin{array}{ccc} & \textit{stop} & \textit{run} & \textit{shock} \\ \textit{stop} & -0.132 & 0.008 & 0.124 \\ \textit{run} & 0.281 & -1.329 & 1.049 \\ \textit{shock} & 0 & 19.77 & -19.77 \end{array} \end{array}$$

(for details, and 95% confidence intervals, see SM).

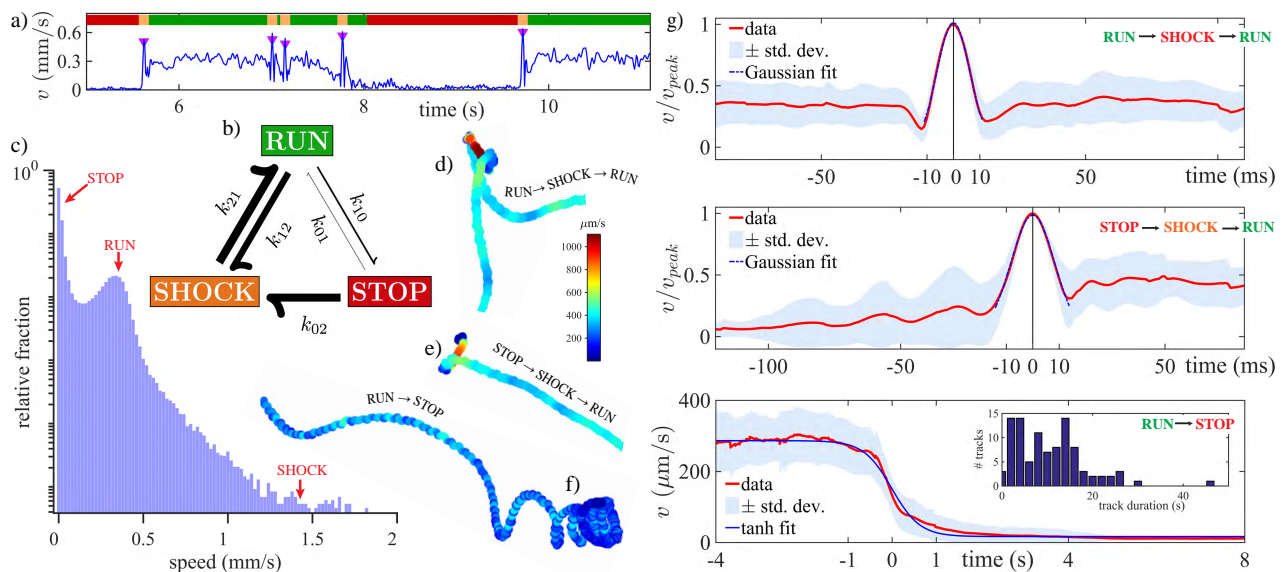


FIG. 3. Gait transitions. (a) Instantaneous speed $v(t)$ is partitioned into three states (0: stop, 1: run, 2: shock). Peaks, at downward triangles, correspond to shocks. (b) Permissible gait bifurcations are indicated by arrows (weighted by transition probability). (c) Probability density distribution of speeds indicates proportionality of dwell times in each state. (d-f) Trajectories of 3 characteristic transition sequences. (g) Superimposed and averaged v -timseries exhibit pulse-like maxima when shocks are involved, but much longer decay if converting from runs to stops. Inset: histogram of track durations.

In total, $\mathcal{O}(10^4)$ s of cumulative recordings (individual track durations 0.5 – 80 s) were analysed, from which 1,377 distinct pairwise transitions were obtained from 233 cells. Waiting times were estimated from diagonal entries $-1/q_{ii}$: stop: 7.60 ± 0.75 s, run: 0.75 ± 0.03 s, shock: 0.05 ± 0.002 s (uncertainties are std. errors). The process admits an embedded Markov chain for discrete jump times, with entries $\{k_{ij}, i \neq j\}$ analogous to chemical reaction rates, which represent the probability of transitioning from $i \rightarrow j$ conditioned on a transition occurring ($\sum_j k_{ij} = 1, \forall i$). Here $k_{ii} = 0$ (no self-transitions), and $k_{01} = 0.0582, k_{02} = 0.9418, k_{10} = 0.2112, k_{12} = 0.7888, k_{20} = 0$ and $k_{21} = 1.0000$ (Fig. 3b). Every state is positive recurrent and the process is irreducible. While run \Rightarrow shock bifurcations occur readily, the direct reaction shock \rightarrow stop is not possible. The network is weakly reversible, not reversible [14], and detailed balance is clearly violated (as is the Kolmogorov flux criterion: $k_{01}k_{12}k_{20} \neq k_{02}k_{21}k_{10}$). The model predicts an equilibrium distribution $\pi(\text{stop}, \text{run}, \text{shock}) = (0.6666, 0.3126, 0.0208)$. From a histogram of speeds (for a larger dataset which also includes tracks with no transitions), we estimated the relative dwell times in each state: (68.6%, 30.8%, 0.6%), according to cut-offs of $0 \sim 40, 40 \sim 500, > 500 \mu\text{m/s}$ (Fig. 3c), which is similar to $\{\pi_i\}$: with discrepancies arising due to subjectivity in choice of cut-off, and prevalence of short-duration tracks.

Gait-switching can greatly affect free-swimming trajectories. Fig. 3d-f zooms in on three primary sequences permitted by Fig. 3b: run \rightarrow shock \rightarrow run, stop \rightarrow shock \rightarrow run, and run \rightarrow stop. Typically for photosynthetic

unicells, forward swimming is helical with a variable pitch superimposed onto self-rotation. Tracks comprise low-curvature portions due to runs, and sharp turns due to rapid conversion of flagellar beating and transient reversal during shocks (Fig. 2d). Canonical runs decelerate from $\sim 400 \mu\text{m/s}$ to full-stop, by sequentially deactivating subsets of flagella (SM), the ensuing torque imbalance gradually increases track asymmetry and curvature (Fig. 3f). Gait-switching requires two very disparate timescales (Fig. 3g): an ultrafast, millisecond, timescale for bifurcations to and from shocks, but a much slower one for entry into stop states. The former is reminiscent of neuronal spiking while the latter is akin to decay of leakage currents. For the first two sequences, the mean is well-fit to a sharply peaked Gaussian ($\sigma = 8.6$ ms, 11.6 ms respectively), whereas run to stop conversions follow a switch-like profile $A \tanh [(x - x_0)/\tau]$ with $\tau = 640$ ms.

The stopped state can be maintained for up to minutes, before the next restart (Fig. 4). While cell body motion is negligible (sub-pixel variance in centroid displacement: $\sigma_{\delta C} = 0.0253 \mu\text{m}$), significant flagellar activity persists (SM and Movie). More surprisingly, we deduce using optical analysis that flagellar tip fluctuations can even be oscillatory! This highly unusual mode may be related to (the much faster) hyperoscillations of reactivated sperm flagella, where the noisy dynamics may be signatures of individual dynein oscillations [15]. Emergence of global limit-cycle oscillations in the flagella is Hopf-like.

In addition to effecting directional reorientation and sensing [16], the shock gait serves another key physiological function: to enable avoidance of obstacles

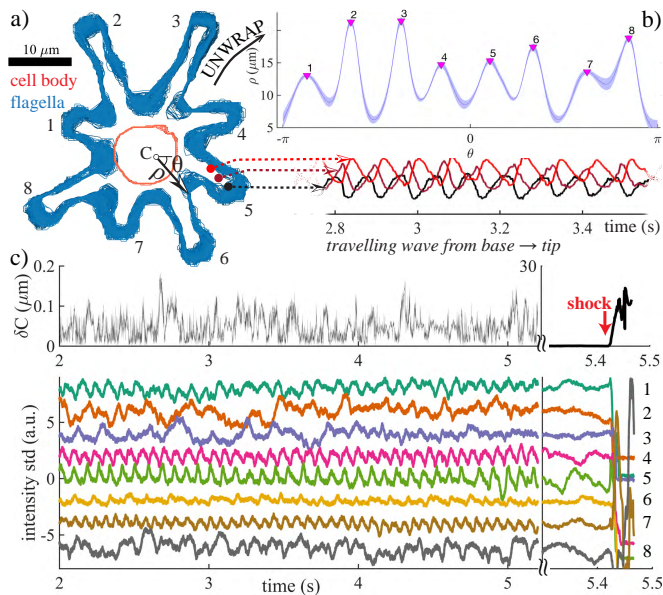


FIG. 4. Arrested, yet still ‘beating’. a) Cell boundaries (with or without flagella) in the stop state are tracked. b) The unwrapped flagellar envelope exhibits μm -fluctuations. Traveling waves, inferred from image intensity changes, propagate outwards from base to tip (inset). c) Centroid fluctuations are sub-pixel, random, but flagellar tips display robust oscillations (e.g. flagella 4,5). Later, activation of full-amplitude beating occurs simultaneously in all flagella (shock).

upon direct mechanical contact. Compared to *Chlamydomonas*, whose flagella display a certain load-response [6, 13, 18, 19], *P. octopus* possess a much heightened mechanosensitivity, where the same downstream pathways leading to *spontaneous* shocks can be activated by touch, to produce *stimulated* shocks that are identical in morphology and dynamics to those described earlier (Fig. 2,3). Fig. 5 shows an example of a moving cell colliding with a cell at rest: cell 1 contacts cell 2 multiple times but triggers a shock in cell 2 only when the perturbation is large enough. For a non-beating flagellum

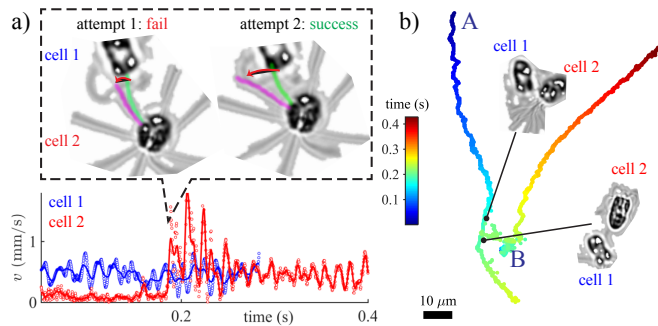


FIG. 5. Mechanosensitivity: a direct cell-cell collision. a) Contact with only one flagellum is sufficient to trigger a shock, depending on stimulus strength. b) Cell 1 (at A) approaches an initially stationary cell 2 (at B), induces shock in the latter.

with bending rigidity $EI = 840 \text{ pN}\mu\text{m}^2$ [17] we estimate the contact force $F = 3EI \cdot \delta/L^3$ from the measured tip deflection in the two cases: fail: $\sim 3.0 \text{ pN}$, success: $\sim 6.6 \text{ pN}$. Signal transduction from the distal point of contact must have occurred within milliseconds.

The unusual motility of *P. octopus* is a significant departure from known classical strategies. Peritrichous enteric bacteria rotate rigid flagellar helices one way or another to cause runs and tumbles, producing a two-state, paradigmatic strategy for prokaryotic chemotaxis and gradient sensing based on stochastic switching between directed swimming and random reorientation [20]. The freshwater alga *C. reinhardtii* displays a eukaryotic version of this, swimming an in-phase breaststroke [21–23] but turning sharply when biflagellar synchrony is lost (‘phase drift’) [24]. Other bacteria species adopt alternative strategies [25–27], e.g. the monotrichous *V. cholerae* undergoes a run-reverse-flick motion where flagellar hook elasticity is key. Contrastingly, the mechanism of enslavement of *P. octopus* swimming to its flagellar dynamics is neither due to motor reversal at the base of the flagellum (as in *E. coli*) nor to loss of biflagellar synchronization (as in *C. reinhardtii*), but rather to a total conversion of beating waveform along the flagellum axoneme proper.

These algae offer rare insight into the bifurcations between different modes of beating in the *same* organelle. Identifying principal modes of beating (ciliary, flagellar, or quiescent) with (run, shock or stop) states, we adopted a natural framework that is liberated from assumptions of specific prototypical gaits (breaststroke, trot, etc). Patterns of flagellar actuation even during ‘run’ phases are diverse and species-specific [4], and environmental stimuli can elicit further changes [18, 30]. The *P. octopus* shock, while identifiable with the stimulus-induced (light, mechanical) avoidance reaction of *C. reinhardtii* and *S. similis*, is importantly only one component of a tripartite repertoire, is more than an order of magnitude shorter in duration, and occurs spontaneously. Our three-state classification therefore does not purport to incorporate the totality of gaits but rather sheds new light on the physiology of gait control. By exploring the statistics of gait transitions, we demonstrated that the gait-switching process, and not just flagellar beating itself [31], operates far from equilibrium – thereby providing a route to enhanced biological sensitivity [32].

The discoveries that flagellar activity in *P. octopus* exhibits rapid activation but slow deactivation, and that apparently quiescent flagella undergo small-amplitude oscillations, have great implications for beat emergence and motor coordination in eukaryotic flagella [28–30]. The millisecond shock timescale facilitates rapid removal from predators or obstacles, analogously to the escape response of ciliates [11]. More generally, depending on the species, flagella type, and number, the ways of achieving motion, no motion, or change of motion are diverse. The purple bacterium *B. photometrium* has a sudden

light-induced reaction (the Schreckbewegung reaction, or ‘fright movement’) [33], whereas sensory inputs that inhibit/enhance the firing rate of a ‘twiddle generator’ [34] can alter the directionality of bacterial flagellar motors. The cilia of a more advanced phylum – ctenophores – rely on neurons to switch between oscillatory/non-oscillatory states [35]. As important sensory appendages in animals [13, 36], rapid transduction of signal must likewise be an essential attribute of mammalian cilia. Thus, in a very primitive unicellular alga, we may have found an evolutionary precedent for the kind of rapid signalling from a distance that, billions of years hence, would come to characterize the key physiological functions of mammalian cilia.

Financial support is acknowledged from Magdalene College Cambridge through a Junior Research Fellowship (KYW), and Senior Investigator Award 097855MA from the Wellcome Trust (REG).

-
- [1] Aristotle, “*De Incessu Animalium* (on the gait of animals),”.
- [2] K. G. Pearson, *Ann Rev Neurosci* **16**, 265 (1993).
- [3] P. Holmes, R. J. Full, D. Koditschek, and J. Guckenheimer, *Siam Rev.* **48**, 207 (2006).
- [4] K. Y. Wan and R. E. Goldstein, *P. Natl. Acad. Sci. USA* (2016).
- [5] J. L. Salisbury, *J. Protozool.* **35**, 574 (1988).
- [6] G. Quaranta, M. Aubin-Tam, and D. Tam, *Phys. Rev. Lett.* **115** (2015).
- [7] G. Klindt, C. Ruloff, C. Wagner, and B. M. Friedrich, *Arxiv*, arXiv:1703.03355 (2017).
- [8] O. Moestrup and T. Hori, *Protoplasma* **148**, 41 (1989).
- [9] We take “ciliary” to mean the large-amplitude asymmetric beat exhibited by most cilia (e.g. epithelial) where the beat cycle partitions into distinct power and recovery stroke phases, and “flagellar” to mean the symmetric undulatory beat of sperms.
- [10] P. Sartori, V. F. Geyer, A. Scholich, F. Julicher, and J. Howard, *Elife* **5**, e13258 (2016).
- [11] R. Eckert, *Science* **176**, 473 (1972).
- [12] G. B. Witman, *Trends Cell Biol.* **3**, 403 (1993).
- [13] K. Fujiu, Y. Nakayama, A. Yanagisawa, M. Sokabe, and K. Yoshimura, *Curr. Biol.* **19**, 133 (2009).
- [14] D. Anderson and T. Kurtz, *Stochastic Analysis of Biochemical Systems*, Mathematical Biosciences Institute Lecture Series (Springer International Publishing, 2015).
- [15] S. Kamimura and R. Kamiya, *Nature* **340**, 476 (1989).
- [16] F. Peruani and L. G. Morelli, *Phys. Rev. Lett.* **99**, 010602 (2007).
- [17] G. Xu, K. S. Wilson, R. J. Okamoto, J. Y. Shao, S. K. Dutcher, and P. V. Bayly, *Biophysical Journal* **110**, 2759 (2016).
- [18] K. Y. Wan and R. E. Goldstein, *Phys. Rev. Lett.* **113**, 238103 (2014).
- [19] G. Klindt, C. Ruloff, C. Wagner, and B. M. Friedrich, *Phys. Rev. Lett.* **117**, 258101 (2016).
- [20] H. C. Berg and D. A. Brown, *Nature* **239**, 500 (1972).
- [21] D. L. Ringo, *J. Cell. Biol.* **33**, 543 (1967).
- [22] J. S. Guasto, K. A. Johnson, and J. P. Gollub, *Phys. Rev. Lett.* **105**, 168102 (2010).
- [23] K. Y. Wan, K. C. Leptos, and R. E. Goldstein, *J. Roy. Soc. Interface* **11**, 20131160 (2014).
- [24] M. Polin, I. Tuval, K. Drescher, J. P. Gollub, and R. E. Goldstein, *Science* **325**, 487 (2009).
- [25] K. M. Taute, S. Gude, S. J. Tans, and T. S. Shimizu, *Nat. Commun.* **6**, 8776 (2015).
- [26] K. Son, J. S. Guasto, and R. Stocker, *Nat. Phys.* **9**, 494 (2013).
- [27] L. Xie, T. Altindal, S. Chattopadhyay, and X.-L. Wu, *P. Natl. Acad. Sci. USA* **108**, 2246 (2011).
- [28] D. Oriola, H. Gadelha, and J. Casademunt, *Roy. Soc. Open Sc.* (2017).
- [29] P. V. Bayly and K. S. Wilson, *J. Roy. Soc. Interface* **12**, UNSP 20150124 (2015).
- [30] U. B. Kaupp and L. Alvarez, *Eur. Phys. J-Spec. Top.* **225**, 2119 (2016).
- [31] C. Battle, C. P. Broedersz, N. Fakhri, V. F. Geyer, J. Howard, C. F. Schmidt, and F. C. MacKintosh, *Science* **352**, 604 (2016).
- [32] Y. Tu, *P. Natl. Acad. Sci. USA* **105**, 11737 (2008).
- [33] T. Engelmann, *Arch. Gesam. Physiol. Mensch Tiere* (1883).
- [34] H. C. Berg, *Ann. Rev. Biophys. Bioeng.* **4**, 119 (1975).
- [35] S. L. Tamm, *Invertebr. Biol.* **133**, 1 (2014).
- [36] M. Delling, A. A. Indzhukulian, X. Liu, Y. Li, T. Xie, D. P. Corey, and D. E. Clapham, *Nature* **531**, 656 (2016).

Run stop shock, run shock run: Spontaneous and stimulated gait-switching in a unicellular octoflagellate

SUPPLEMENTAL MATERIAL

Kirsty Y. Wan and Raymond E. Goldstein

*Department of Applied Mathematics and Theoretical Physics, Centre for Mathematical Sciences,
University of Cambridge, Wilberforce Road, Cambridge CB3 0WA, United Kingdom*

In the following, we give further details of some of the techniques and analyses employed in the main text.

1. A pusher-puller transition

For free-swimming microalgae, the motion of the cell is tightly coupled to the motion of the flagella [2, 3]. Our results show that sharp reorientations in swimming trajectories in *P. octopus* are elicited by dramatic conversion of flagellar beating waveforms. Cells have a well-defined length-width aspect ratio β which we determined from a large sample population $\mathcal{O}(100)$ of cells to be $\beta = 1.9 \pm 0.2$.

Importantly $\beta \neq 1$ which allows us to distinguish the longitudinal and transverse directions of an organism moving in the focal plane. The anterior and posterior poles are defined by the user on frame t_0 of each movie, but tracked automatically thereafter.

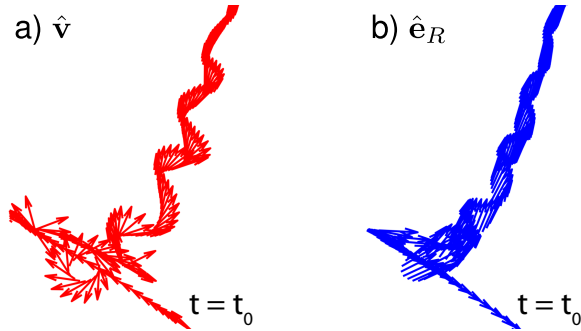


FIG. S1. Cell orientation versus direction of swimming: the puller-pusher dichotomy.

For a given trajectory, we obtain 2D coordinates for the anterior $\mathbf{A}_i(t)$, posterior $\mathbf{P}_i(t)$, and centroid of the cell $\mathbf{C}_i(t)$, at discrete times indexed by t_0, t_1, t_2, \dots , ($\Delta t = t_{j+1} - t_j$). From this we take the instantaneous swimming direction $\hat{\mathbf{v}}$ and the instantaneous orientation $\hat{\mathbf{e}}_R$ to be

$$\mathbf{v}(t_j) = \frac{\mathbf{C}(t_{j+1}) - \mathbf{C}(t_{j-1})}{2\Delta t} \quad (1)$$

$$\mathbf{e}_R(t_j) = \mathbf{A}(t_j) - \mathbf{P}(t_j) \quad (2)$$

and define $\hat{\mathbf{v}} = \mathbf{v}/\|\mathbf{v}\|$, $\hat{\mathbf{e}}_R = \mathbf{e}_R/\|\mathbf{e}_R\|$.

In Figure S1 the two quantities are plotted following the same trajectory, starting at $t = t_0$, which shows a cell switching from a backward swimming, pusher-like shock gait to a forward, puller-like run gait. The recovery from a flagellar to ciliary beat is concomitant with a continuous modulation of the swimming direction. At this magnification (63x water immersion objective, Zeiss Plan Apochromat), we see that $\hat{\mathbf{v}}$ is everywhere tangent to a helical run trajectory (due to self-rotation).

2. Tracing moving boundaries

At sufficiently high magnification, it is possible to distinguish the cell body from the flagella bundle. For this, we take advantage of the differences in image intensity features between the cell body and flagella. The algorithm was written in MATLAB with the aid of the Image Processing Toolbox (version 9.5).

Fig. S2 shows the morphing outer boundary of the organism (exterior of the flagella) as it transitions from a stopped state (red), undergoes a shock response (amber), before moving off in a new direction (green). The exterior boundary was detected from the raw intensity image using the Sobel method (Fig. S2b) and by morphological dilation and erosion of the edge-like features, as required (Fig. S2c). Further, to detect the inner boundary (cell body only), we restrict to and quantize the sub-image bounded by this external border (Fig. S2d) into a darker central region and peripheral pixels that are not part of the background. Finally, the image is binarized, selecting only the central region (Fig. S2e).

3. Transition Probabilities between states

The instantaneous swimming speed ($v(t) = \|\mathbf{v}(t)\|$ defined above) is an efficient means of segregating the observed dynamics into the three states of interest. A combination of signal processing criteria (e.g. filtering by minimum peak height, minimum peak to peak separation etc) was used to convert a typical v -timeseries (e.g. Fig. 3a) into a discretized signal that takes on only one of three values: 0 = stop, 1 = run, 2 = shock.

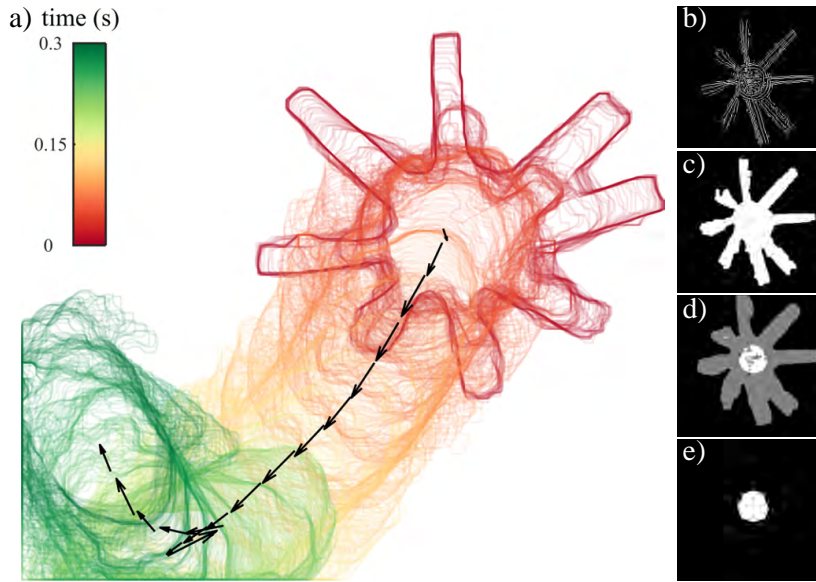


FIG. S2. a) The flagellar envelope is traced for a cell starting from a stopped state. Arrows follow the direction of motion of the cell body. The processing algorithm devised for delineating the inner and outer cell boundaries, is summarized in b-e). and in turn used for computing λ (Fig. 2c, main text).

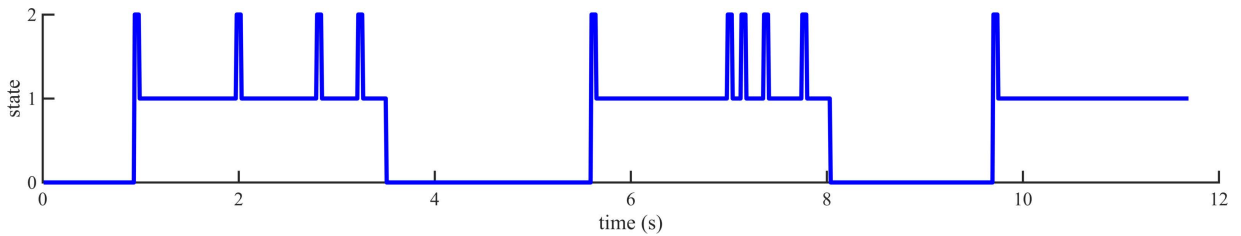


FIG. S3. A sample track showing discrete transitions between three states (0 = stop, 1 = run, 2 = shock), is obtained by discretizing the instantaneous cell swimming speed.

Model formulation In order to analyse the likelihood of gait-switching, we shall model the underlying stochastic process generating the empirical data as a continuous time, discrete space Markov chain for states $X(t) \in \{0, 1, 2\}$. In reality X is measured at a succession of times discretized by imaging frame-rate, which we assume to be sufficient to provide the necessary temporal resolution. Multiple tracks are then sampled to obtain longitudinal data in the form $\{X_{mn}, m = 1, 2, \dots, N, n = 1, 2, \dots, m_N\}$, for a total of N -tracks corresponding to different cells, and in which each track m is observed for m_N frames.

Next, we wish to compute the transition intensity

$$q_{ij}(s, t) = \lim_{s \rightarrow t} \frac{\mathcal{P}(X(t) = j | X(s) = i)}{t - s}, \quad (3)$$

which represents the risk of q_{ij} of moving into state j at time t starting from state i at time s . We shall assume the Markov property, that is for $t_0 < t_1 < \dots < t_n$,

$$\begin{aligned} \mathcal{P}(X(t_n) = i_n | X(t_0) = i_0, \dots, X(t_{n-1}) = i_{n-1}) \\ = \mathcal{P}(X(t_n) = i_n | X(t_{n-1}) = i_{n-1}), \end{aligned} \quad (4)$$

and that the process is homogeneous: $\mathcal{P}(X(t) = j | X(s) = i) = \mathcal{P}(X(t - s) = j | X(0) = i) =: p_{ij}(t - s)$. The instantaneous probability distribution $P_i(t) = \mathcal{P}(X(t) = i)$ ($\sum_i P_i(t) = 1$) is then completely determined by the initial distribution $p_0 = P_i(0)$ and the infinitesimal transition rate matrix $Q = \{q_{ij}\}$. Off diagonal entries $q_{ij} > 0$ for $i \neq j$ are given by eqn (4), while diagonal entries

$$q_{ii} = - \sum_{j \neq i} q_{ij}.$$

The transition matrix $P = \{p_{ij}\}$ satisfies the Chapman-Kolmogorov equations $p_{ij}(s, t) = \sum_k p_{ik}(s, u)p_{kj}(u, t)$, and the matrix differential equation $dP/dt = P(t)Q$ (forward equation), with solution

$$P(t) = \exp(Qt) = \sum_{k=0}^{\infty} \frac{Q^k t^k}{k!}. \quad (5)$$

Defining the sequence $\{T_n\}_{n \in \mathbb{N}}$ of jump times

$$T_{n+1} = \inf\{t \geq T_n | X(t) \neq X(T_n)\}, \quad (6)$$

then the sojourn times $S_n = T_n - T_{n-1}$ are exponentially distributed with rate $\lambda = -q_{ii}$, i.e.

$$\mathcal{P}(S_n \leq t) = 1 - \exp(q_{ii}t),$$

and moreover this new state is $j \neq i$ with probability

$$\lim_{h \rightarrow 0} \frac{\mathcal{P}(X(t+h) = j | X(t) = i)}{\mathcal{P}(X(t+h) \neq i | X(t) = i)} = -\frac{q_{ij}}{q_{ii}}. \quad (7)$$

Then the stochastic matrix given by:

$$\tilde{p}_{ij} = \begin{cases} 1 & (q_i = 0; j = i) \\ 0 & (q_i = 0; j \neq i) \\ -q_{ij}/q_{ii} & (q_i \neq 0; j \neq i) \\ 0 & (q_i \neq 0; j = i) \end{cases} \quad (8)$$

defines a transition matrix for an *embedded Markov chain*, where the \tilde{p}_{ij} are the probabilities that given a transition occurs, the state moves from i to j . The embedded chain has no self-transitions.

Recall that a finite-state irreducible Markov chain is positive recurrent, so in this case we expect a unique stationary distribution π to exist, and to satisfy:

$$\lim_{t \rightarrow \infty} P(t) = \mathbf{1}\pi.$$

The process is *time-reversible* iff it is in detailed balance

$$\pi_i q_{ij} = \pi_j q_{ji}$$

Results We sampled a total of $N = 233$ tracks each containing at least one transition event, with mean track duration 11.5 s and maximum track duration 78.2 s. The data is reshaped so that there is only one row per transition, corresponding to observations for a given cell. Next we sub-sample so that only jump-times are retained $\{X_{mn_k} : t_{n_k} \text{ corresponding to jump times } T_k^m\}$ in the sense of eqn (6). A total of 1377 pairwise transitions were observed, with the following frequencies

| | <i>stop</i> | <i>run</i> | <i>shock</i> |
|--------------|-------------|------------|--------------|
| <i>stop</i> | 0 | 0.005 | 0.070 |
| <i>run</i> | 0.085 | 0 | 0.317 |
| <i>shock</i> | 0 | 0.523 | 0 |

The data was fitted to the above Markov state model using the R-software package `msm` [1] to obtain maximum likelihood estimates for unknown parameters. Let $\{T_i\}$ be the total time the process is observed in each state, N_i the total number of observed transitions from state i , and N_{ij} the number of transitions from i to j . We can use eqn (7) to initialize the Q -matrix, where N_{ij}/N_i is an estimate for $-q_{ij}/q_{ii}$ and T_i/N_i can be used to estimate the mean waiting time in state i (expected to be $-1/q_{ii}$). Thus, $\hat{q}_{ij} = N_{ij}/T_i$.

The following Q -matrix was obtained (together with 95% confidence intervals)

| | <i>stop</i> | <i>run</i> | <i>shock</i> |
|--------------|--------------------------------|--------------------------------|-----------------------------------|
| <i>stop</i> | -0.13166 (-0.159709, -0.10854) | 0.00767 (0.003446, 0.01707) | 0.12399 (0.101617, 0.15129) |
| <i>run</i> | 0.28075 (0.234222, 0.33652) | -1.32937 (-1.444803, -1.22315) | 1.04862 (0.954768, 1.15169) |
| <i>shock</i> | 0 | 19.76936 (18.376811, 21.26743) | -19.76936 (-21.267428, -18.37681) |

(9)

We can also compute the transition matrix $P(t)$, which estimates the transition probabilities at different times.

$$P(0.01) = \begin{matrix} & \begin{matrix} stop & run & shock \end{matrix} \\ \begin{matrix} stop \\ run \\ shock \end{matrix} & \begin{bmatrix} 0.9987 & 0.0002 & 0.0011 \\ 0.0028 & 0.9878 & 0.0095 \\ 0.0003 & 0.1782 & 0.8215 \end{bmatrix} \end{matrix} \quad (10)$$

$$P(0.1) = \begin{matrix} & \begin{matrix} stop & run & shock \end{matrix} \\ \begin{matrix} stop \\ run \\ shock \end{matrix} & \begin{bmatrix} 0.9870 & 0.0074 & 0.0055 \\ 0.0267 & 0.9299 & 0.0434 \\ 0.0152 & 0.8163 & 0.1685 \end{bmatrix} \end{matrix} \quad (11)$$

$$P(1) = \begin{matrix} & \begin{matrix} stop & run & shock \end{matrix} \\ \begin{matrix} stop \\ run \\ shock \end{matrix} & \begin{bmatrix} 0.8902 & 0.0992 & 0.0106 \\ 0.2201 & 0.7389 & 0.0410 \\ 0.2109 & 0.7477 & 0.0414 \end{bmatrix} \end{matrix} \quad (12)$$

where time is measured in units of seconds, and stochas-

tic matrices are truncated to 4 decimal places. The above has interesting interpretations, for instance the shock state is confirmed to be the most transient, since the probability of arriving from a shock state to another shock state drops from 0.8215 at time $t = 0.01$ s down to 0.1685 at $t = 0.1$ s.

As $t \rightarrow \infty$, the rows of P converge to:

$$\pi(\text{stop}, \text{run}, \text{shock}) = (0.6666, 0.3126, 0.0208).$$

The MLEs for diagonal entries \hat{q}_{ii} , by the Markov assumption, give estimates (together with standard errors) for the mean waiting time in state i :

$$\begin{aligned} \{E(T_i) = -1/\hat{q}_{ii}\}(\text{stop}, \text{run}, \text{shock}) \\ = (7.60 \pm 0.75, 0.75 \pm 0.03, 0.05 \pm 0.002). \end{aligned}$$

Futhermore, the transition matrix for the embedded

Markov process [eqn (8)] is given by

$$\tilde{q}_{ij} = \begin{matrix} & \begin{matrix} stop & run & shock \end{matrix} \\ \begin{matrix} stop \\ run \\ shock \\ /, . \end{matrix} & \begin{bmatrix} 0 & 0.0582 & 0.9418 \\ 0.2112 & 0 & 0.7888 \\ 0 & 1.0000 & 0 \end{bmatrix} \end{matrix}$$

Finally, we estimate the relative time spent in each state within a certain time window (t_0, t_1) , here taken to be 10 s, coincident with the average duration of an observed track. Note this is different from the expected waiting times – which considers only single stays. For

$$\frac{1}{t_1 - t_0} \int_0^{10} P(t) dt = (stop : 0.71, run : 0.27, shock : 0.02).$$

In the long time limit as $t_1 - t_0 \rightarrow \infty$ we recover the stationary distribution π_i .

4. An(other) example of a single-cell trajectory

A cell experiencing multiple shocks in quick succession makes several sharp turns (Fig. S3). Given a 2D set of trajectory coordinates $r(t) = (x_1(t), x_2(t))$ obtained from tracking of cell centroids, we measure instantaneous speeds $v = \|\mathbf{v}(t)\|$ as before (recall Eqn. 1). Writing $\mathbf{v}(t) = v(\cos(\theta), \sin(\theta))$, we define the angular speed $|\omega|$ (where $|\cdot|$ denotes absolute value):

$$\omega(t) = \frac{1}{2\Delta t} (\theta(t + \Delta t) - \theta(t - \Delta t)).$$

However, the orientation variable $\theta(t)$ is especially sensitive to noise, and derivative computations become problematic at high frame rates.

We resolve this problem by obtaining a track simplification via a recursive Ramer-Douglas-Peucker algorithm [4] with a relative tolerance of $0.5/\gamma$, where γ is the calibration for the number of μm s per pixel on the image frame. Briefly, the algorithm recursively removes points that lie within the given tolerance of the line defined by the end points obtained from the previous iteration. The output polygonal line is then a simplification of the original trajectory, with the advantage that sharp discontinuities are usually preserved. ω can then be determined from the simplified track (Fig. S5).

5. Velocity pulse alignment

A few additional comments are in order regarding the signal alignment procedure used in Fig. 3g. In each case, the alignment must be determined relative to a well-defined feature of interest. The first two sequences (run \rightarrow shock \rightarrow run or stop \rightarrow shock \rightarrow run) contain shock events, which correspond to highly reproducible

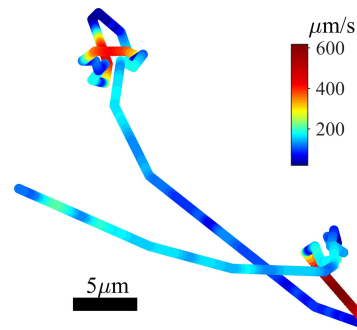


FIG. S4. The cumulative effect of shocks on swimming trajectories.

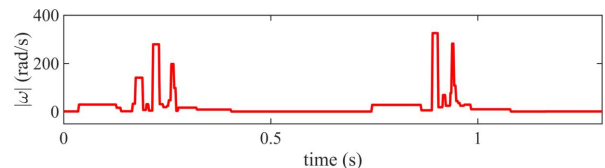


FIG. S5. Angular speed during shocks can reach several hundred radians per second.

pulse-like signatures in the time series of speeds, which provide a natural reference point. All signals are then time-shifted so that the origin is at these local minima. However, we should note that cells can undergo significant out-of-plane reorientations during shocks so that the maximum speed reached is highly variable. For instance any centroid motion of a cell that reverses perpendicularly to the focal plane will not be detected in a 2D projection. Future work could seek to improve tracking fidelity by extending the imaging to 3D.

In Fig. 3g, we focused on determining a common *timescale* for shocks by rescaling the i th sequence by v_{max}^i , that is, $t = 0$ where $v_{max}^i = \max_{t_{min} \leq t \leq t_{max}} v^i(t)$. The most accurate estimate for the maximum speed reached during shocks is $1,712 \pm 392 \text{ m/s}$ (see Fig. 2b), accounting for only those individuals for whom shocks occurred in the focal plane.

However there are no such peaks in run \rightarrow stop transitions. Instead, we use the derivative of the velocity, obtained by first filtering the signal with a lowpass filter.

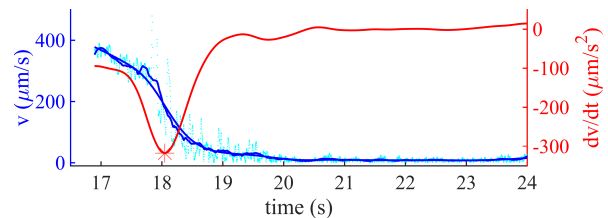


FIG. S6. Alignment of velocities for run \rightarrow stop transitions using local maxima in *acceleration*. Peak *deceleration* occurs at the time indicated by the asterisk.

The decay response from run speed to full stop exhibits a tanh-like or hyperbolic profile, centred about the time point where the derivative is most negative (Fig. S6).

6. Flagellar activation versus flagellar deactivation

In the main text, we have discussed the separation in timescales between a very fast activation and a much slower deactivation. Here, we show further how activation generally involves simultaneous bifurcation to full-amplitude oscillations but yet in the reverse process the flagella do not stop beating at the same time.

Partial deactivation. A cell undergoing a run \rightarrow stop transition requires several seconds to slow down to rest from full speed. The continuous convergence of $\theta(t)$ to a fixed orientation angle is shown on Fig. S7. The trajectory loops several times before terminating, as a result of the torque imbalance produced by a subset of flagella that would continue to beat well after the remainder have already stopped.

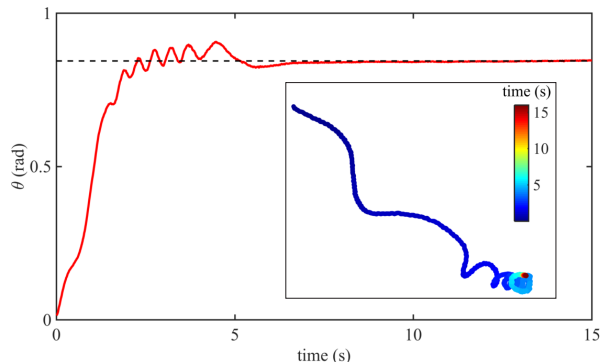


FIG. S7. Evolution of orientation angle over time, with corresponding trajectory (inset).

Simultaneous activation. In Fig. S8 we follow the exterior boundary traced by the flagella during a stop \rightarrow shock transition. Within 20 ms, the boundary has morphed from the red outline to the green. In particular, by identifying peaks corresponding to the 8 flagella (from unwrapped polar angle), we can obtain the trajectories of each of the flagella tips during this process (dark blue to light indicates increasing time coordinate).

Slow small-amplitude ‘oscillations’. Finally, recall that the eight flagella shown in Fig. 4 (main text), to varying degrees, exhibit oscillations. To investigate if there is *global* periodicity, Instead of measuring all possible permutations of interflagellar cross-correlations, we consider the total area spanned by the flagellar envelope ($487 \pm 9.88 \mu\text{m}^2$), which fluctuates over time. The existence of a $12 \sim 13$ Hz oscillation is evident from the area auto-correlation function $C_{area}(\tau) = \langle X(t)X(t+\tau) \rangle_{\tau}$. Oscillations in $C_{area}(\tau)$ is indicative of an *intracellular* origin for the ‘globally’ quivering state – signalling to the

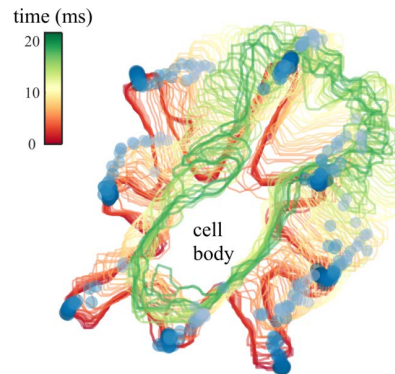


FIG. S8. Simultaneous activation of all flagella at shock onset.

flagella bundle collectively, as opposed to an *intraflagellar* phenomenon occurring in a single flagellum only.

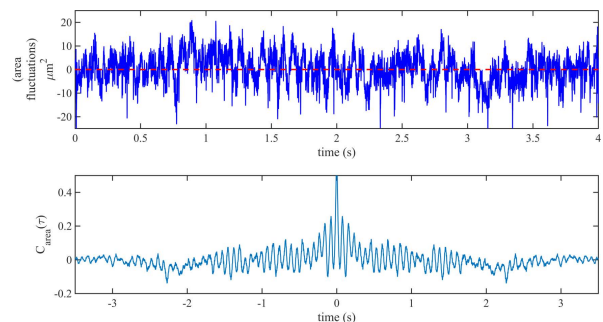


FIG. S9. Area fluctuations (a) and its auto-correlation function (b) for a cell observed during the stop state.

7. Captions for supplemental movies

MovieSM1 threesequences Examples of the three primary sequences discussed in the text, namely run \rightarrow shock \rightarrow run, stop \rightarrow shock \rightarrow run, and run \rightarrow stop.

MovieSM2 quiverandshock A cell observed during the stop state. Despite no cell body motion, the flagella continue to ‘quiver’. Remarkably, these fluctuations are not random, but exhibit very small-amplitude, slow oscillations.

MovieSM3 collision Stimulated initiation of a shock reaction in a *P. octopus* cell, initially at rest, due to mechanical contact with another cell.

-
- [1] G.B. Witman, **1993**, 403 (1993).
 - [2] O. Moestrup, *Protoplasma* **148**, 41 (1989).
 - [3] C.H. Jackson, *Journal of Statistical Software* **38**, 1 (2011).
 - [4] W. Schwanghart, *Line Simplification* version 1.4, MATLAB Central File Exchange, (2010).